Accepted Manuscript

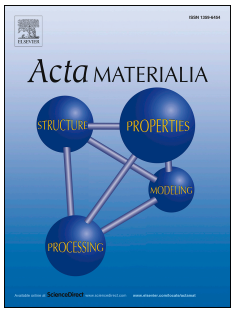

Fabrication, characterisation and modelling of uniform and gradient auxetic foam sheets

O. Duncan, T. Allen, L. Foster, T. Senior, A. Alderson

PII: S1359-6454(17)30004-6

DOI: 10.1016/j.actamat.2017.01.004

Reference: AM 13466

To appear in: *Acta Materialia*

Received Date: 27 October 2016

Revised Date: 3 January 2017

Accepted Date: 4 January 2017

Please cite this article as: O. Duncan, T. Allen, L. Foster, T. Senior, A. Alderson, Fabrication, characterisation and modelling of uniform and gradient auxetic foam sheets, *Acta Materialia* (2017), doi: 10.1016/j.actamat.2017.01.004.

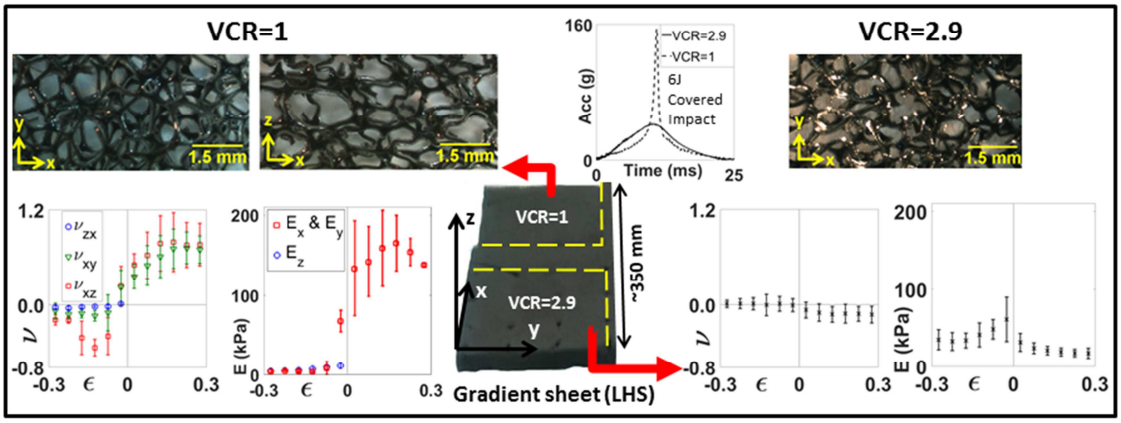

Fabrication, characterisation and modelling of uniform and gradient auxetic foam sheets

O. Duncan [a], T. Allen [b], L. Foster [c], T. Senior [c], A. Alderson [a,*]

[a] *Materials and Engineering Research Institute, Faculty of Arts, Computing, Engineering and Sciences, Sheffield Hallam University, Howard Street, Sheffield S1 1WB UK.*

[b] *Sports Engineering Research Team, School of Engineering, Faculty of Science & Engineering, Manchester Metropolitan University, John Dalton Building, Chester Street, Manchester M1 5GD, UK.*

[c] *Centre for Sports Engineering Research, Faculty of Health and Wellbeing, Sheffield Hallam University, Broomgrove Teaching Block Street, Sheffield S10 2LX, UK.*

***** Corresponding author (Email: A.Alderson@shu.ac.uk)

Abstract

Large sheets of polyurethane open-cell foam were compressed (or stretched) using pins and a conversion mould whilst undergoing thermal softening and controlled cooling. Sheets (final dimensions 355 x 344 x 20 mm) were fabricated with uniform triaxial compression, with and without through-thickness pins, and also with different compression regimes (uniform triaxial compression or through-thickness compression and biaxial planar tension) in opposing quadrants. The samples fabricated under uniform triaxial compression with and without pins exhibited similar cell structure and mechanical properties. The sheets fabricated with graded compression levels displayed clearly defined quadrants of differing cell structure and mechanical properties. The graded foam quadrants subject to triaxial compression displayed similar cell structure, tangent moduli and negative Poisson's ratio responses to the uniform foams converted with a similar level of triaxial compression. The graded foam quadrants subject to through-thickness compression and biaxial planar tension displayed a slightly re-entrant through-thickness cell structure contrasting with an in-plane structure resembling the fully reticulated cell structure of the unconverted parent foam. This quadrant of graded foam displayed positive and negative Poisson's ratios in tension and compression, respectively, accompanied by high and low in-plane tangent modulus, respectively. The strain-dependent mechanical properties are shown to be fully consistent with expectations from honeycomb theory. The triaxially compressed quadrants of the graded sheet exhibited ~4 times lower peak acceleration than quadrants with through-thickness

compression and biaxial planar tension in 6 J impact tests using a steel hemispherical drop mass.

Keywords

Auxetic, Poisson's Ratio, Foams, Mechanical Properties, Gradient

1. Introduction

Open cell auxetic polyurethane (PU) foams [1] display negative Poisson's ratio (PR) and have potential in a range of applications. These include apparel [2], personal protective equipment [3,4,5], crash barriers [5], car/plane seats [6], anti-vibration gloves [7], cleanable/tuneable filters and controlled delivery devices [8,9]. For impact applications, for example, auxetic foams exhibit reduced peak force [3,4,5] and displacement [10], and increased energy absorption [11,12] under impact loading.

Auxetic foams are typically fabricated by combined triaxial compression in a metal mould and thermal softening [1,3, 13,14]. Alternative softening processes for PU foam use solvents [15] or compressed carbon dioxide [16]. A vacuum bag can be used in place of a rigid mould [17]. The combination of compression and softening changes the open cell foam structure from an initially quasi-regular arrangement of cells comprising nearly straight ribs connected at junctions into a more dense and tortuous cell structure [1] through buckling of the ribs and rotation of the junctions [18]. Subsequent removal of the thermal load (and/or solvent or carbon dioxide) while maintaining the mechanical load then fixes the foam in the converted 're-entrant' structure responsible for the auxetic effect [1,19]. Evidence of buckled ribs has also been reported in commercial felted PU and melamine foams, with the felted melamine foam found to display auxetic behaviour under flat plate impact [10].

The compression applied via the conversion process is a significant contributor to modifying the cellular structure and mechanical properties of the produced auxetic foams [3,20,21,22]. Imposing uniform and equal compression (within reasonable limits) along each

of the three principal directions produces isotropic auxetic foams [1]. Auxetic behaviour is typically realised, with varying magnitude of negative PR, for volumetric compression ratios (VCR – ratio of unconverted-to-converted foam volume) in the range 2-5 [10,23]. Applying different compression levels along different axes produces auxetic foams displaying anisotropic mechanical properties (PRs and Young's moduli) [24,25]. Employing different levels of compression in different regions produces foams displaying gradient structure and mechanical properties. Graded compression levels have been achieved by inserting a sample having a different unconverted shape to the compression mould to produce a longitudinally-gradient foam with gradient cellular structure and negative and positive PR regions [26]. The gradient effect can be produced in discrete homogeneous segments (by inserting a pre-converted foam having uniformly thick and uniformly thin regions into a uniform cross-section cuboidal mould) [26] or in a gradually varying manner along the length (tapered cuboidal pre-converted foam into a uniform cross-section cuboidal mould) [27]. An alternative approach to achieving graded compression levels exploits the cellular nature of the foam structure, allowing the insertion of pins to constrain regions of foam by different amounts during conversion. Pins have been used to produce a coaxial radially-gradient foam cylinder displaying an auxetic annular sheath region surrounding a positive PR inner core [27].

Issues with foam compression in the mould include (unintentional) non-uniform compression throughout the bulk of the monolith. Non-uniform compression can lead to surface creasing [13], over compression towards the outer corners and edges, and under compression towards the centre of the foam [4,28]. Under compression results in cellular structure which is less tortuous than typical auxetic foam and closer to its unconverted state [4]. These issues become more apparent as the size of the foam increases. Strategies to reduce surface creasing include using a lubricant to line the walls of the mould and the use of

spatulas to smooth out the creases whilst in the mould [13]. For monoliths approaching seat cushion size (~5 cm thick, ~38 cm planar dimension), the force required to insert the foam into the mould becomes an issue for the compression levels required to achieve auxetic behaviour [29]. Applying compression using an adjustable mould [29,30] or through multiple conversion cycles with increasing compression [13] can make it easier to insert the foam into the mould. Adjustable moulds [29,30] are complex to design and the multi-stage compression method requires different sized moulds [13].

For large area foams having thin through-thickness dimension (relative to in-plane dimensions), it becomes difficult to achieve the required in-plane compression without creasing or even folding of the foam during insertion into the compression mould. A vacuum bag and 'half mould' process has produced 10 mm thick foam sheets of arbitrary curvature displaying anisotropic auxetic behaviour in the plane of the sample. Negative PRs of -0.15 through the thickness and below -1 in some in-plane directions were reported for the 'half mould' samples [17]. Uniaxial compression between flat or curved plates, rather than in a fixed compression mould, has been used to produce surface crease-free flat and curved samples, respectively, with thickness as low as 2-3mm [31]. In this case the auxetic effect is evident through the thickness, with negative PR values as low as -3 reported, but auxetic behaviour was not observed in the plane of the converted foam.

There is surprisingly little prior literature comparing the prediction of strain-dependent mechanical properties from structural models with experimental data for auxetic foams. An analytical model for isotropic auxetic foam based on a polyhedron cell gave good agreement with experimental PR vs strain data for auxetic copper foam [23]. Predictions from a 2D analytical model of a hexagonal honeycomb deforming solely by flexure of the ribs were compared with FE model predictions based on a 3D elongated rhombic dodecahedron, but neither variation with strain nor comparison with experimental data were undertaken [32].

A multiple-mechanism 3D elongated rhombic dodecahedron analytical model has been developed and stress-strain predictions compared to experimental auxetic and conventional foam data, but a PR vs strain comparison was not performed [33].

Auxetic foams are, then, exemplary systems to explore processing-structure-properties relationships in cellular solids and offer the potential to produce carefully tailored properties for a range of applications. Further improvements in the processing of auxetic foams are, however, required. It is within this context that we have recently developed the use of pins further to constrain the foam during the conversion process, providing a means of local internal compression control to complement the global applied external compression from the mould [5,34]. This work investigates the efficacy of pins for control of planar compression in the thermo-mechanical conversion method [1] to produce large (355 x 344 x 20 mm) homogeneous sheets of auxetic foam. Additionally, we use pins to apply non-uniform planar compression to produce foams displaying in-plane gradient cellular structure and mechanical properties. This latter development extends the previous work on longitudinally- and radially-gradient auxetic foams to include planar-gradient auxetic foam sheets. We undertake impact testing of the gradient foam to demonstrate the production of a one-piece foam sheet having regions of distinctly different impact response. Finally, by considering projections of foam structure in specific planes as idealised 2D honeycombs [19], we extend the established analytical model for deformation of 2D hexagonal honeycombs via simultaneous flexing, rotation and stretching of the honeycomb ribs [35] to allow predictions with strain. Comparison of the experimental structure and properties data with model predictions is undertaken.

2. Methods

2.1. Foam fabrication

A multi-stage thermo-mechanical process [13], adopted from previous studies on the same foam and range of sizes [4,5,10,34], was applied to open cell PU R30FR foam (Custom Foams). Foam sheets (508 x 491 x 28.5 mm) were compressed into a metal mould (internal dimensions 355 x 344 x 20 mm), with the rise direction through the thickness. A Linear Compression Ratio (LCR, initial length/final length) of 1.43 was thus applied in all 3 principal directions to two sheets corresponding to a VCR of 2.9. One uniform sheet utilised a square array of 36 steel pins of diameter 3.2 mm inserted through the thickness of the unconverted foam, with a typical spacing of 71.5 mm prior to insertion into the mould and 50 mm after insertion (Figure 1). The other sheet was fabricated without pins. A coordinate system was defined whereby z is through the sample thickness (or rise direction in unconverted samples) and x and y are the two planar axes (Figure 1a). [**Insert Fig 1 here]**

A sheet was also fabricated with non-uniform compression, having quadrants with different VCRs separated by a transition region (Figure 1b). The unconverted sample was cut to size with a retractable-blade knife using a laser cut acrylic sheet template. Through-thickness pins applied planar compression or tension to different regions. To impose a VCR of 1, an LCR of 0.84 (i.e. linear extension of 19%) was applied in both planar directions (pin spacing ~ 42 mm prior to insertion, and 50 mm in the mould) in two diagonally opposite quadrants. An LCR of 1.43 was imposed in the remaining quadrants (pin spacing ~ 71.5 mm prior to insertion, and 50 mm in the mould), providing equal compression in each direction with a VCR of 2.9 to match the uniform sheets. In comparison to the uniform sheets, 28 additional pins were used 10 mm from the mould edge to apply tension and control transition regions.

The compression method comprised (only steps 3 & 4 apply without pins):

1) Pins were positioned in the unconverted foam by passing them through holes (maximum clearance = 0.1 mm) in a 5 mm thick laser cut acrylic sheet covering the sample. The acrylic sheet was then removed.
2) The pins were then inserted through holes in the lower box like section of the metal mould (Figure 1a) and into corresponding holes in a wooden guide block positioned below (Figure 1c & 1d), working from the centre to the edges of the mould.
3) All corners and edges of the sample were tucked into place around the edge of the mould. Horizontal rods were used to hold the foam in place while creases were removed (Figure 1c).
4) The flat lid was put into place (locating the pins in holes in the lid in the case of pinned samples) and the horizontal rods (Figure 1c) were removed as compression was applied. The lid was held in place by inserting three 3.2 mm diameter steel rods through holes in the walls of the mould (Figure 1d).

The closed mould assembly was subject to two heating stages at 180°C (25 and 15 minutes respectively) in a conventional oven (MCP Tooling Technologies LC/CD), followed by annealing at 100°C for 20 minutes in a separate oven (Genlab PWO/600), similar to previous work with this foam [3,4,5,10,34]. After each heating phase the mould was removed from the oven. Uniform sheets were taken out of their mould and gently stretched by hand to avoid adhesion of the cell ribs, with any pins removed after the 1st heating phase and not returned. Pins remained in place, to maintain tension, for both heating phases of the gradient sheet, before removal for annealing. This sheet was agitated between heating phases by compressing and releasing the lid. All samples were gently stretched before annealing.

2.2. Impact testing of the non-uniform sheet

Prior to dissection for structural and mechanical characterisation, the non-uniform sheet was covered unbonded with a 2 x 350 x 350 mm polypropylene (PP) sheet (Direct Plastics, PPH/PP-DWST-Homopolymer). Impacts were based on the British Standard for

cricket pads [36] and previous work [4,34], with the sample resting on a flat rigid surface rather than a curved anvil. Impacts were performed at 6 J by dropping a 2.095 kg, 72 mm diameter hemispherical hammer from 292 mm. Acceleration was recorded at 50 kHz with a hammer-mounted accelerometer (Analog devices, ADXL001-500g). The sheet was impacted in the z direction close to the centre of 2 quadrants with different VCRs (Figure 2a). Three impacts were performed at each location, alternating between the imposed VCR=1 and 2.9 quadrants. The interval between impacts was ≥7.5 minutes, equating to ≥15 minutes between repeats in the same location. Three shells were used, 2 impacts per shell, each on opposing corners. Impacted quadrants were not used for further testing.

2.3. Foam characterisation

Three cubes were cut from each of the distinct quadrants of the non-uniform foam (Figure 2a). For the uniform sheet 3 cubes were cut from 5 different regions (15 total), corresponding to: 1) corners, 2) positions along the edge, 3) positions 10 mm from the edge, 4) an intermediate region between 50 mm and 100 mm from the edge and 5) a region within 75 mm of the centre (example positions shown in Figure 2b). Three cuboidal samples were cut from each of the uniform and distinct quadrants of the non-uniform foams, aligned along each of the in-plane directions, and also along an in-plane diagonal. Additionally, 6 cuboidal samples were cut from a larger block of unconverted foam, with 2 aligned along each axis. Densities of all dissected samples were measured using weighing scales (accurate to 0.001g) and digital vernier calipers (accurate to 0.01 mm). The final VCR, determined from the ratio of converted to unconverted densities (30 kg/m^3, centre of supplier stated density range of 28-32 kg/m^3 and checked using unconverted samples) was compared to the imposed value, to see if the intended amount of compression was achieved.

Mechanical characterisation comprised of tensile tests (strain rate = 0.0042 s^{-1}) on all cuboidal samples, and compression tests (strain rate = 0.0083 s^{-1}) on the cubic samples, to

50% engineering strain in an Instron 3367 machine fitted with a 500 N load cell. The movements of white-headed pins set into the front face of each sample, filmed with a Sony Handycam HFR-CX250, were tracked using an in-house Matlab R2015a (MathWorks) script for strain determination (frame rate of 5 Hz and resolution of 720 by 540 pixels). PR was obtained from linear regression of lateral true strain vs axial true strain. Tangent modulus was obtained from linear regression of stress vs axial engineering strain from the marker tracking. The cuboidal test specimens were each subject to 4 tensile tests along their length, with the sample being rotated 90°between tests. This allowed tests with the x-y and x-z faces alternately oriented towards the camera, so that 1 in-plane and 1 through-thickness PR per specimen were measured in tests 1 and 2, and also in tests 3 and 4. The starting orientation was randomised between samples since it is known that the properties can vary with repeat testing. Hence results are presented for the average directional PRs between samples from tests 1 and 2, and from tests 3 and 4. The cubic samples were each tested 3 times in compression: test 1 - loading through the thickness, test 2 - in-plane loading direction with x-z plane facing the camera, and test 3 - in-plane loading with x-y plane facing the camera.

[Insert Fig 2 here]

Tested cubic samples were cut into thin (~1 mm) slices using a razor blade and placed on a white background to obtain microscopic images of cellular structure using a Stereoscope (LECIA S6D).

2.4. Analytical model

A simplified reconciliation of the cellular structure and mechanical properties data is undertaken by representing the foam structures in the x-z and x-y planes as idealised 2D hexagonal honeycombs [19]. We use analytical expressions previously developed for the on-axis and off-axis mechanical properties of hexagonal honeycombs deforming via simultaneous flexing, hinging (rotation) and stretching of the ribs of the cellular structure

[35]. The full set of elastic constants expressions, adapted from [35], is reproduced in the Supplementary Material.

For the prediction of the variation of mechanical properties with applied strain, the loading strain for loading along the x direction was calculated using:

$$\varepsilon_x(\phi) = \ln\left(\frac{l_{xz}\cos\theta_{xz}-\delta_{xz}\sin\theta_{xz}}{l_{xz(0)}\cos\theta_{xz(0)}}\right)\cos^2\phi + \ln\left(\frac{h_{xz}+l_{xz}\sin\theta_{xz}+\delta_{xz}\cos\theta_{xz}}{h_{xz(0)}+l_{xz(0)}\sin\theta_{xz(0)}}\right)\sin^2\phi \quad (1)$$

where h and l are 'vertical' (aligned along z) and 'oblique' honeycomb rib lengths, respectively, δ is the deflection of the oblique rib due to flexing, θ is the angle of the oblique ribs with the horizontal (x) axis, and the subscript 'xz' applied to the geometrical parameters denotes they are in the x-z plane. The geometrical parameters are shown in the schematic insert in Figure 7a later. The subscript '(0)' denotes the undeformed value of the associated geometrical parameter and, for loading along x, $h_{xz} = h_{xz(0)}$. The variation of oblique rib length l_{xz} and deflection δ_{xz} with rib angle θ_{xz} under an x-directed load was derived using a similar approach to that used in the Nodule-Fibril model for microporous polymers [37]:

$$l_{xz}^2 = -\frac{2K_h}{K_s}\ln\left(\frac{sin\theta_{xz}}{sin\theta_{xz(0)}}\right) + l_{xz(0)}^2 \quad (2)$$

$$\delta_{xz} = \frac{K_h}{K_f}\frac{(\theta_{xz}-\theta_{xz(0)})}{l_{xz}} \quad (3)$$

In Eqns (2) and (3), K_s, K_h and K_f are force constants governing the rib stretching, hinging and flexure modes of deformation, and K_h/K_s and K_h/K_f have been assumed to remain constant throughout deformation. Any particular mechanism becomes increasingly dominant as the value of its force constant decreases. Full details of the derivation of Eqns (1)-(3), and similar expressions for a z-directed load, are given in the Supplementary Material.

3. Results

The mean measured VCR of the uniform sheet converted with pins was 2.63 ±0.10 (cuboidal samples) and 2.96 ±0.42 (cubic samples), which was similar to 2.53 ±0.04 (cuboidal) and 2.86 ±0.51 (cubic) for the sheet without pins and the imposed value of 2.9.

Cuboidal samples from the non-uniform sheet had a mean VCR of 2.98 ±0.33 in the triaxially compressed region and 1.22 ±0.01 in the region with imposed biaxial planar tension.

Micrographs show the regular polyhedral cellular structure of the unconverted foam, with elongation in the rise direction [19] (Figure 3a & 3b). The planar (x-y) structure of the quadrant of the gradient foam converted with biaxial planar tension and through-thickness compression (VCR = 1, Figure 3c) is similar to the unconverted parent foam planar structure (Figure 3a). In the through-thickness (x-z) plane, this region of foam has a slightly re-entrant structure consisting of vertically compressed, partially buckled cells (Figure 3d). Through-thickness and planar micrographs of the triaxially compressed quadrant (VCR = 2.9) of the gradient foam (Figure 3e & 3f) both show a dense three dimensional re-entrant cell structure typical of auxetic foam [1] and similar to the uniformly compressed samples as intended. Through-thickness pins left holes in foam sheets (hole diameter ≈ pin diameter), surrounded by small creases (~10 mm long sloping down into the holes to a depth of <5 mm) (Figure 3g). Random creasing (length <100 mm, depth ~ 5 mm) was evident in the sheet converted without pins. Creases or folds were not present in the region with applied planar tension in the gradient sheet, which exhibited defined boundaries between areas with different VCRs (Figure 3h). **[Insert Fig 3 here]**

There was no clear difference in PRs or tangent moduli between samples cut at different orientations from converted sheets (Figure 2), so these are displayed and discussed together. The unconverted foam shows the established deformation characteristic of open cell foams, undergoing lateral contraction under axial tension, and lateral expansion under axial compression (Figure 4a). The strain-dependent PRs determined from the negative of the slope of the strain-strain data are, thus, positive for the unconverted foam and attain highest values at the highest tensile strain and near zero values at the highest compressive strains (Figure 4b), in agreement with previous work [22,23]. There is evidence for anisotropy in tensile PR

response for the unconverted foam, with the systematic trend of $\nu_{zx} > \nu_{xz} > \nu_{xy}$, consistent with the structural anisotropy (rise direction parallel to z axis). **[Insert Fig 4 (and Fig4b.csv, Fig4c.csv and Fig4d.csv) here]**

The foam converted with uniform triaxial compression also displays the previously reported response of lateral expansion under axial tension, and lateral contraction under axial compression (Figure 4a), for foam converted in a similar manner. This corresponds to essentially isotropic negative PR response of larger magnitude ($\nu \sim -0.2$) in tension than compression ($\nu \sim 0$, Figure 4b). Conversion with and without pins exhibited little difference in the PR response of foams converted with uniform triaxial compression (Figure 4b).

Turning to the foam converted with non-uniform compression, it is clear that a gradient foam in terms of mechanical response in addition to structure, noted above, has been produced through the use of pins and foam of a different shape to the mould. The VCR = 2.9 region displays very similar PR vs axial strain (Figure 4c) data to the foam sheets converted with uniform triaxial compression (Figure 4b), as intended. The VCR = 1 region undergoes lateral contraction under axial tension (Figure 4a), similar to the unconverted foam, although the magnitudes of the positive PRs are higher for the VCR = 1 region of the gradient foam (Figure 4c). The positive PR response is maintained under low (<5%) strain axial compression (Figure 4a and 4c). However for compressive strains greater than 5%, the VCR = 1 region undergoes lateral contraction under axial compression (Figure 4a) and, thus, transitions to negative PR behaviour (Figure 4c). The through-thickness plane shows large anisotropy in this case, with $\nu_{xz} \sim -0.6$ and $\nu_{zx} \sim 0$ at compressive loading strains ~10-15%. The tensile PR response of the VCR = 1 region of the gradient foam was found to be sensitive to repeat testing, decreasing in magnitude with increasing repeat testing (Figure 4d).

The stress-strain responses of the unconverted foam and the VCR=1 quadrant of the gradient sheet include the presence of a plateau onset under 5% compression for the

unconverted foam (Figure 5a). The triaxially compressed samples exhibit increased elastic resilience (longer linear stress-strain response) under compression (Figure 5a). The triaxially compressed foam stress-strain data display lower tensile slope and higher compression slope, corresponding to lower tensile and higher compressive Young's moduli, respectively (Figure 5b), than the unconverted foam. The elastic anisotropy and isotropy of the unconverted foam and triaxial compression foam, respectively, are again evident in the Young's moduli data. No clear differences were observed in the Young's modulus data for samples converted under uniform triaxial compression with and without pins (Figure 5b). **[Insert Fig 5 (and Fig5b.csv, Fig5c.csv and Fig5d.csv) here]**

The sheets converted with uniform triaxial compression display the intended similar Young's modulus response to the VCR = 2.9 quadrant in the gradient foam (Figures 5b and 5c, respectively). In the VCR = 1 region, the gradient foam displays similar Young's moduli trends to the unconverted foam. However, the tensile E_x has been increased by a factor of ~3 for the VCR = 1 region of the gradient foam (tensile E_x ~ 150 kPa, Figure 5c) compared to the unconverted foam (tensile E_x ~ 50 kPa, Figure 5b). As with the PR response, the Young's modulus response of the VCR = 1 region of the gradient foam is susceptible to repeat testing, reducing with the 1st and 2nd tests, before stabilising under the 3rd and 4th tests (Figure 5d).

Figure 6 shows the median impact acceleration/time trace in each region of the gradient sheet. The VCR = 2.9 quadrant exhibited a mean peak acceleration ~4 times lower than the VCR = 1 region, which appeared to "bottom out" under impact (characterised by a sharp increase in acceleration). Mean peak accelerations were 43 g (s.d. = 0.1 g) and 162 g (s.d. = 47 g) for the VCR = 2.9 and 1 regions, respectively (Figure 6). **[Insert Fig 6 (and Fig6.csv) here]**

To model the mechanical properties using the 2D hexagonal honeycomb expressions (Supplementary Material), we introduce a combined force constant parameter: $K_{hf} =$

$K_h K_f / [K_h + K_f]$. The force constants can be related to the geometry and mechanical properties of the ribs (and their junctions) [35]. For the parameters used in this work, K_{hf}/K_s ~ 0.004 to 0.04, depending on whether hinging occurs via bending or shearing of the rib junction [35] (Supplementary Material). To show the effect of processing-induced changes in foam structure on the effective PR, Figure 7a shows the ν_{xz} expression and the predicted ν_{xz} vs θ_{xz} trends for K_{hf}/K_s = 0 (flexing/hinging), 0.004, 0.04 and ∞ (stretching), when h_{xz} = 1.2, l_{xz} = 1 and rib thickness b_{xz} = 0.2. These parameters provide a slight elongation of the cell along the rise (z) direction when θ_{xz} = 30° (see cell schematics below θ_{xz} axis in Figure 7a), and are taken as the simplified 2D representation of the 3D unconverted foam structure in the x-z plane (Figure 3b). The curves for finite values of K_{hf}/K_s lie between the stretching and flexing/hinging extremes, with the (lower) K_{hf}/K_s = 0.004 curve closest to the flexing/hinging case. Points A, B and C on the K_{hf}/K_s = 0.004 curve in Figure 7a correspond to honeycombs qualitatively approximating the observed cellular structures in the x-z plane, shown in Figure 3, for the unconverted foam and VCR = 2.9 and 1 gradient foam quadrants, respectively. Points A and B lie in regions of clear positive and negative predicted values of ν_{xz}, respectively, whereas ν_{xz} varies dramatically (from negative through zero to positive values) for small variation in θ_{xz} around point C. **[Insert Fig 7 (and Fig7a.csv and Fig7b.csv) here]**

As an example of predicted off-axis properties, Figure 7b shows the variation of ν_{xz} for rotation about the y axis, normal to the x-z plane, by angle φ when θ_{xz} = 0° (see insert to Figure 7b) for K_{hf}/K_s = 0.004 and 0.04. This example, then, approximates the VCR = 1 quadrant of the gradient foam. $\nu_{xz}(\varphi)$ = 0 when φ = 0 and 90°, is positive when 0 < φ < 90°, and is symmetric about φ = 0 and 90°. The maximum value of $\nu_{xz}(\varphi)$ increases, and is approached more rapidly, as φ increases from 0 for the lower K_{hf}/K_s value, occurring at φ = 26 and 15° when K_{hf}/K_s = 0.04 and 0.004, respectively. A range of 5 < φ < 15° produces

predicted positive $\nu_{xz}(\varphi)$ values for K_{hf}/K_s = 0.04 and 0.004 of similar magnitude to the experimental ν_{xz} value at zero strain (Figures 7b and 4c, respectively).

For comparison with the experimental strain-dependent mechanical properties we use Equations (1) and (2) to plot the predicted variation of $\nu_{xz}(\varphi)$ with loading strain for the VCR = 1 quadrant of the gradient foam (Figure 8a, dashed curve). The predictions use h_{xz} = 1.2, l_{xz} = 1, b_{xz} = 0.2, θ_{xz} = -0.1°, φ = 10° and K_{hf}/K_s = 0.004 (K_f/K_h = 9, K_s/K_h = 225). The value of φ = 10° lies in the middle of the range identified above, and the (arbitrary) near-zero choice of $\theta_{xz(0)}$ = -0.1° was employed since Equation (2) is indeterminate when $\theta_{xz(0)}$ = 0. There is no component of the applied x-directed force to cause flexing or rotation of the ribs of length l_{xz} when they are aligned along the x direction (i.e. when $\theta_{xz(0)}$ = 0). The model of concurrent rib hinging/flexure with stretching is then invalid in this case. The model is, however, valid for non-zero values of $\theta_{xz(0)}$, and predicts trends in broad agreement with the experimental ν_{xz} vs ε_x data (filled diamonds, Figure 8a) when $\theta_{xz(0)}$ = -0.1. **[Insert Fig 8 (and Fig8a.csv and Fig8b.csv) here]**

We next consider the same x-z plane, and geometrical and force constant parameters, but now due to loading along the z direction. The $\nu_{zx}(\varphi)$ vs $\varepsilon_z(\varphi)$ trend (dot-dash line in Figure 8a) is in good agreement with the experimental compression data (filled squares). No experimental tensile data are available for comparison.

The x-y plane comparison between ν_{xy} vs ε_x predictions (dotted line) and experimental data (filled triangles) is also shown in Figure 8a. The x-y plane model predictions employ h_{xy} = l_{xy} = 1, b_{xy} = 0.2 and θ_{xy} = 30° since the cell structure in the x-y plane of the VCR = 1 quadrant of the gradient foam is similar to that of the unconverted foam (Figures 3a,c) and they replicate the symmetrically equivalent x- and y-directed mechanical properties. No rotation of axes was considered for the predicted x-y plane properties (i.e. φ = 0°). The ν_{xy} vs ε_x model predictions follow the experimental trends reasonably well when employing a value

of K_{hf}/K_s = 0.3 (by reducing K_s/K_h to 3). This is significantly higher than the value used in the x-z plane predictions, and corresponds to a stiffening of the rib flexing and/or hinging mechanisms relative to the rib stretching mechanism in the x-y plane.

The model parameters used in the PR predictions also produce Young's moduli (normalised to the respective zero strain E_x value) vs strain trends in reasonable agreement with experiment (Figure 8b). There are E_x model predictions from each of the x-z and x-y plane parameters, with the trends from the x-z plane parameters in particular reproducing an enhanced drop off in E_x in compression.

4. Discussion

We have shown here that through-thickness pins can be used to control local compression levels to fabricate large gradient foam sheets containing regions with dramatically different structures and properties. The controlled production of desired auxetic regions (within pre-defined quadrants and with VCR = 2.9) has been shown. The VCR = 1 regions display a novel transition from positive to negative PRs moving from tensile to compressive loading (Figure 4c), and possess highly anisotropic cellular structure (Figure 3c & 3d) and mechanical properties (Figure 4c, 4d, 5c & 5d). The use of pins for local control of compression or tension in the thermo-mechanical conversion process used in this paper can be extended to the alternative solvent [15] and compressed carbon dioxide [16] foam conversion routes.

The observed structures and mechanical properties of the unconverted and uniform triaxial compression-converted foams are consistent with previous reports [12,28,38]. Uniform samples fabricated with pins exhibited no clear difference in mechanical properties to those without. For the production of homogeneous foams, pins are then expected to be most beneficial when applying compression to thinner sheets than those fabricated here (where folding can prevent uniform planar compression) and thicker monoliths to aid

insertion into the mould and minimise density gradients/variation. The conversion of thicker samples may also benefit from the addition of an orthogonal set of pins in a modified mould. Metallic pins, such as those used here, are expected to aid heat conduction through thicker samples.

The PRs and Young's modulus of the VCR = 1 region of the gradient foam both reduced with repeat testing until stabilising around the 4th test (Figures 4d and 5d). Reduced mechanical properties in both auxetic and conventional open cell PU foams under cyclic loading have been reported previously, with most decrease occurring over the first few loading cycles [39].

When the gradient sheet was impacted in the z direction at 6 J, peak acceleration was ~4 times lower for the VCR = 2.9 region than the VCR = 1 region (Figure 6). In both cases the compressive ν_{zx} ~ 0 (Figure 4c) and so PR cannot account for the different impact responses. It is likely due to the compressive tangent modulus (beyond ~5% compressive strain) being close to zero for the VCR = 1 region (Figure 5c), resulting in the material offering little resistance to the impactor, the sample 'bottoming out' and exhibiting a higher peak acceleration. Nevertheless, the ability to modify impact response in a one-piece foam is demonstrated, leading to potential applications in sport, healthcare and defence apparel requiring localised impact protection (e.g chest and shoulder regions in rugby), for example.

Our extension of the existing model of a hexagonal honeycomb deforming by multiple mechanisms [35] allows predictions as a function of strain, and provides increased insight into the mechanisms giving rise to the experimental foam mechanical properties. Reasonable agreement between experiment and predicted properties is demonstrated for the VCR = 1 quadrant of the gradient foam (Figure 8).

For reasons of brevity, a comparison of model and experimental strain-dependent properties is not reported for the unconverted foam, nor for the foam converted with uniform

triaxial compression or the VCR = 2.9 quadrants of the graded foam. We can, however, qualitatively infer the expected trends from Figure 7a for these cases. Consider, firstly, the structure and properties in the x-z plane of the unconverted foam, indicated by point A at θ_{xz} = 30° and the schematic cell inserts for $\theta_{xz} > 0°$ on the ν_{xz} vs θ_{xz} plot of Figure 7a. Increasing θ_{xz} beyond 30° leads to a narrowing of the cell along the x direction and thus corresponds to a compressive stress ($\sigma_x < 0$) applied in the loading (x) direction. Similarly, decreasing θ_{xz} below 30° corresponds to a tensile stress ($\sigma_x > 0$). In this case, the positive value of ν_{xz} at θ_{xz} = 30° decreases under compression, and increases under tension, and is consistent with the experimental ν_{xz} vs ε_x data for the unconverted foam (Figure 4b).

A similar consideration can be extended to point B (θ_{xz} = -30°) in Figure 7a, assumed to approximate the re-entrant cell structures of the triaxially compressed foam and also the VCR = 2.9 region of the gradient foam (Figure 3f). The predicted negative value of ν_{xz} at θ_{xz} = -30° decreases in magnitude under compression ($\theta_{xz} < -30°$), and increases in magnitude under tension ($\theta_{xz} > -30°$), along x. This is also consistent with the experimental ν_{xz} vs ε_x data for the foam converted under triaxial compression, and the VCR = 2.9 region of the gradient foam (Figures 4b and 4c).

The equivalent honeycomb structure for the x-z projection of the VCR = 1 region of the gradient foam (Figure 3d) corresponds to $\theta_{xz} \sim 0°$. In this case, the reconciliation of the experimental and model data trends required a consideration of the off-axis properties [35]. There is a suggestion that buckling of the ribs in the x-z plane of the VCR = 1 region of the gradient foam may be accompanied by some re-orientation of the pores (insert in Figure 3d), and perfect alignment of the irregular pore structure with the testing direction would be difficult, if not impossible, to achieve in practice in any event. It might be expected, therefore, that some off-axis loading of cells occurs in practice. The value of $\varphi \sim 10°$ required

to reproduce the experimental ν_{xz} value at zero strain (Figures 7b and 4c, respectively) appears reasonable and consistent with Figure 3d.

No rotation of axes was considered (i.e. $\varphi = 0°$) for the x-y plane properties of the VCR = 1 region of the gradient foam, since there is no clear experimental evidence for this from Figure 3c, and isotropic properties are predicted by the model for the undeformed honeycomb in this case. Reasonable agreement with experimental ν_{xy} vs ε_x trends was obtained when employing an apparently high value of $K_{hf}/K_s = 0.3$ in the model predictions. Buckling of ribs in the through-thickness (z) direction was observed following conversion (Figure 3d), and this is not evident in the projection of the structure in the x-y plane (Figure 3c). In which case, hinging may be mediated by (lower stiffness) rib bending in the x-z plane and (higher stiffness, K_{hf} increasing) shearing of junction material in the x-y plane. Additionally, compression along x leads to an increased buckling of the ribs along their length, along with increased rotation out of the x-y plane, both leading to a decrease in their projected length in the x-y plane. This will be a much lower stiffness (K_s decreasing) contribution to the apparent rib stretching mechanism than actual stretching/contraction of the rib material itself. Taken together, these 3D effects lead to the potential for $K_{hf}/K_s >> 0.04$ (the upper limit for deformation due to stretching and shearing of rib material in the 2D system), consistent with the value of $K_{hf}/K_s = 0.3$ required in the model predictions.

5. Conclusions

The cellular structure and mechanical properties of open-cell PU foam can be altered by changing the compression regime applied in the thermo-mechanical conversion process. Control of localised compression can be achieved by employing pins inserted through the foam. Triaxially-compressed sheets fabricated with through-thickness pins exhibited similar properties to those fabricated without pins, suggesting negligible effects due to densification and creasing surrounding pin holes. The pins controlled compression levels effectively to

enable the fabrication of heterogeneous sheets of foam having regions displaying markedly different cellular structure, and mechanical and impact properties. A consideration of projections of the cellular structure in terms of simplified idealised 2D honeycombs deforming via simultaneous flexing, rotation and stretching of the cell ribs can explain the observed mechanical properties reasonably well.

Acknowledgements

Funding: This work was supported by Sheffield Hallam University [ACES Graduate Teaching Associate studentship].

References

[1] R. Lakes, Foam structures with a negative Poisson's ratio, Science 235 (1987) 1038-1040.
[2] M. Bentham, A. Alderson, K.L. Alderson, Garments Having Auxetic Foam Layers, U.S. Patent Application 12/277,457 (2008).
[3] T. Allen, J. Shepherd, T. Hewage, T. Senior, L. Foster, A. Alderson, Low-kinetic energy impact response of auxetic and conventional open-cell polyurethane foams, Phys. Status Solidi B 252 (2015) 1631-1639.
[4] O. Duncan, L. Foster, T. Senior, A. Alderson, T. Allen, Quasi-static characterisation and impact testing of auxetic foam for sports safety applications, Smart Materials and Structures 25 (2016) 054014.
[5] T. Allen, O. Duncan, L. Foster, T. Senior, D. Zampieri, V. Edeh, A. Alderson, Auxetic foam for snow-sport safety devices, Snow Sports Trauma and Safety: Proceedings of the International Society of Skiing Safety 21 (In Press).
[6] A. Lowe, R.S. Lakes, Negative Poisson's ratio foam as seat cushion material, Cellular Polymers 19 (2000) 157-168.
[7] F. Scarpa, J. Giacomon, Y. Zhang, P. Pastorino, Mechanical performance of auxetic polyurethane foam for antivibration glove applications, Cellular Polymers 24 (2005) 253–268.
[8] A. Alderson, J. Rasburn, S. Ameer-Beg, P.G. Mullarkey, W. Perrie, K. E. Evans, An auxetic filter: a tuneable filter displaying enhanced size selectivity or de-fouling properties, Ind. Eng. Chem. Res. 39 (2000) 654–665.
[9] A. Alderson, J. Rasburn, K.E. Evans, Mass transport properties of auxetic (negative Poisson's ratio) foams, Phys. Status Solidi B 244 (2007) 817–27.
[10] T. Allen, N. Martinello, D. Zampieri, T. Hewage, T. Senior, L. Foster, A. Alderson, Auxetic Foams for Sport Safety Applications, Procedia Eng. 112 (2015) 104-109.
[11] C. Ge, A comparative study between felted and triaxial compressed polymer foams on cushion performance, J. Cellular Plastics 49 (2013) 521-533.
[12] J. Lisiecki, T. Błazejewicz, S. Kłysz, G. Gmurczyk, P. Reymer, G. Mikułowski, Tests of polyurethane foams with negative Poisson's ratio, Phys. Status Solidi B 250 (2013) 1988–1995.
[13] N. Chan, K.E. Evans, Fabrication methods for auxetic foams, J. Mater. Sci. 32 (1997) 5945-5953.
[14] P. Pastorino, F. Scarpa, S. Patsias, J.R. Yates, S. Haake, M. Ruzzene, Strain rate dependence of stiffness and Poisson's ratio of auxetic open cell PU foams, Phys. Status Solidi B 244 (2007) 955-965.
[15] J.N. Grima, D. Attard, R. Gatt, R.N. Cassar, A novel process for the manufacture of auxetic foams and for their re-conversion to conventional form, Adv. Eng. Mater. 11 (2009) 533-535.
[16] Y. Li, C. Zeng, Room-temperature, near-instantaneous fabrication of auxetic materials with constant Poisson's ratio over large deformation, Adv. Mater. 28 (2016) 2822–2826.
[17] M. Bianchi, F. Scarpa, M. Banse, C.W. Smith, Novel generation of auxetic open cell foams for curved and arbitrary shapes, Acta Mater. 59 (2011) 686-691.
[18] S.A. McDonald, G. Dedreuil-Monet, Y.T. Yao, A. Alderson, P.J. Withers, In situ 3D X-ray microtomography study comparing auxetic and non-auxetic polymeric foams under tension, Phys. Status Solidi B 248 (2011) 45–51.
[19] L.J. Gibson, M.F. Ashby, Cellular Solids: Structure and Properties, Cambridge University Press, Cambridge, 1999.
[20] M. Bianchi, F. Scarpa, C.W. Smith, Stiffness and energy dissipation in polyurethane auxetic foams, J. Mater. Sci. 43 (2008) 5851-5860.

[21] M. Bianchi, F. Scarpa, C.W. Smith, G.R. Whittell, Physical and thermal effects on the shape memory behaviour of auxetic open cell foams, J. Mater. Sci. 45 (2010) 341-347.
[22] Y.C. Wang, R. Lakes, A. Buttenhof, Influence of cell size on re-entrant transformation of negative Poisson's ratio reticulated polyurethane foams, Cellular Polymers 20 (2001) 373-385.
[23] J.B. Choi, R.S. Lakes, Nonlinear analysis of the Poisson's ratio of negative Poisson's ratio foams, J. Comp. Mater. 29 (1995) 113-128.
[24] F. Scarpa, P. Pastorino, A. Garelli, S. Patsias, M. Ruzzene, Auxetic compliant flexible PU foams: static and dynamic properties, Phys. Status Solidi B 242 (2005) 681–694.
[25] A. Alderson, K.L. Alderson, P.J. Davies, G.M. Smart, The effects of processing on the topology and mechanical properties of negative Poisson's ratio foams, In ASME 2005 International Mechanical Engineering Congress and Exposition (2005) 503-510.
[26] A. Alderson, K.L. Alderson, S.A. McDonald, B. Mottershead, S. Nazare, P.J. Withers, Y.T. Yao, Piezomorphic materials, Macromol. Mater. Eng. 298 (2013) 318-327.
[27] M. Sanami, A. Alderson, K.L. Alderson, S.A. McDonald, B. Mottershead, P.J. Withers, The production and characterization of topologically and mechanically gradient open cell thermoplastic foams, Smart Mater. Struct. 23 (2014) 055016-29.
[28] J. Lisiecki, S. Kłysz, T. Błazejewicz, G. Gmurczyk, P. Reymer, Tomographic examination of auxetic polyurethane foam structures, Phys. Status Solidi B 251 (2013) 314-320.
[29] M.A. Loureiro, R.S. Lakes, Scale-up of transformation of negative Poisson's ratio foam slabs, Cellular Polymers 16 (1997) 349-363.
[30] R.S. Lakes, M.A. Loureiro, International Patent Publication No. WO 99/25530 (1999).
[31] K. Alderson, A. Alderson, N. Ravirala, V. Simkins, P. Davies, Manufacture and characterisation of thin flat and curved auxetic foam sheets, Phys. Status Solidi B 249 (2012) 1315–1321.
[32] K.E. Evans, M.A. Nkansah, I.J. Hutchinson, Auxetic foams: modelling negative Poisson's ratios, Acta Metall. Mater. 42 (1994) 1289-1294.
[33] Y.N.X. Chan, The mechanical properties of auxetic foams. PhD Thesis. University of Liverpool. (1995).
[34] O. Duncan, L. Foster, T. Senior, T. Allen, A. Alderson, A comparison of novel and conventional fabrication methods for auxetic foams for sports safety applications, Procedia Eng. 147 (2016) 384–389.
[35] I. Masters, K. Evans, Models for the elastic deformation of honeycombs, Composite structures 35 (1996) 403-422.
[36] BS 6183-3: 2000. Protective equipment for cricketers-leg protectors for batsmen, wicket-keepers and fielders, and thigh, arm and chest protectors for batsmen. British Standards Institute.
[37] A. Alderson, K.E. Evans, Modelling concurrent deformation mechanisms in auxetic microporous polymers, J. Mater. Sci. 32 (1997) 2797-2809.
[38] J.B. Choi, R.S. Lakes, Nonlinear properties of polymer cellular materials with a negative Poisson's ratio, J. Mater. Sci. 27 (1992) 4678-4684.
[39] A. Bezazi, F. Scarpa, Tensile fatigue of conventional and negative Poisson's ratio open cell PU foams, Int. J. Fatigue 31 (2009) 488–494.

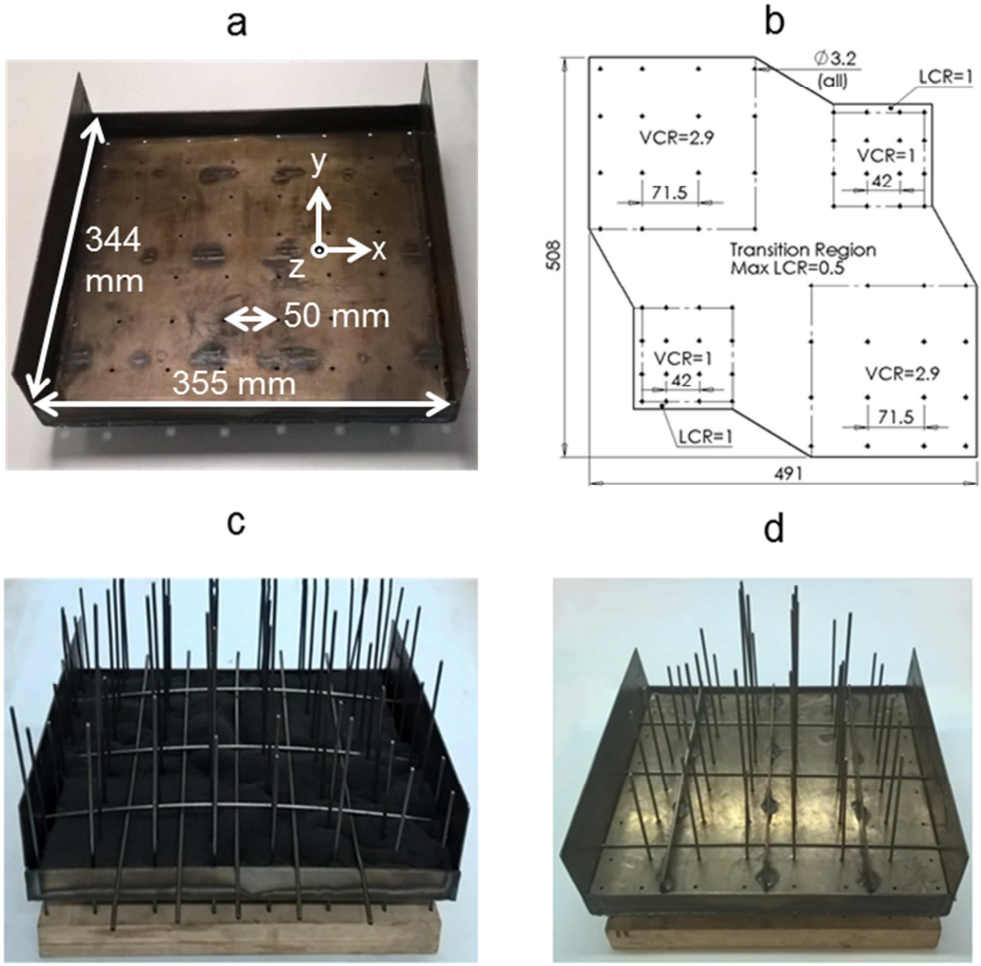

Figure 1: Compression mould. a) Mould lower section, b) Design of acrylic template defining overall shape and pin spacing for the non-uniform sheet (dimensions in mm), c) Assembled lower mould section and pins, with horizontal rods to compress bulges, d) Assembled mould and pins, with horizontal lid to apply through thickness compression.

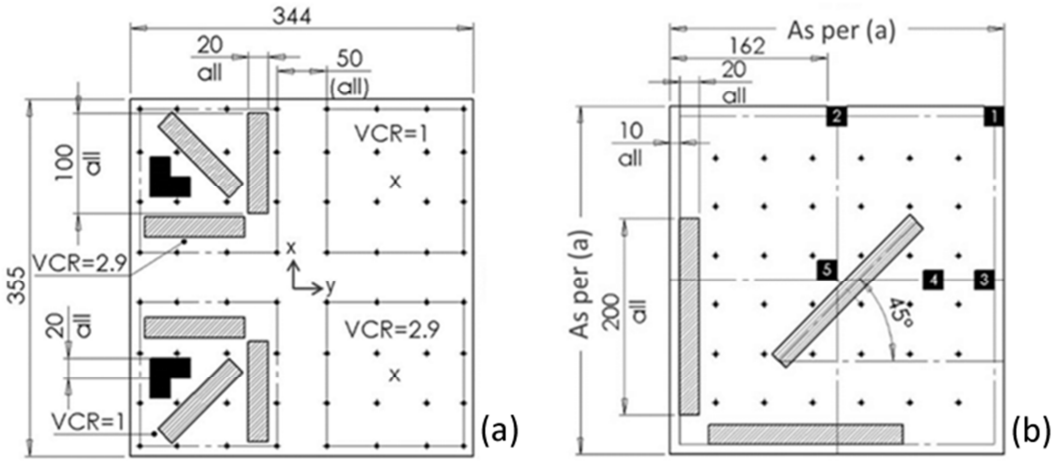

Figure 2: Test sample locations. Tensile (▨) and compression quasi-static test sample locations (■) for: a) Non-uniform sheet (X marks impact locations), b) Uniform compression conversions [1=Corner, 2=edge, 3=outer ring created by pins, 4 = 2nd ring, 5=central two rings]. All dimensions in mm, sheets 20 mm thick.

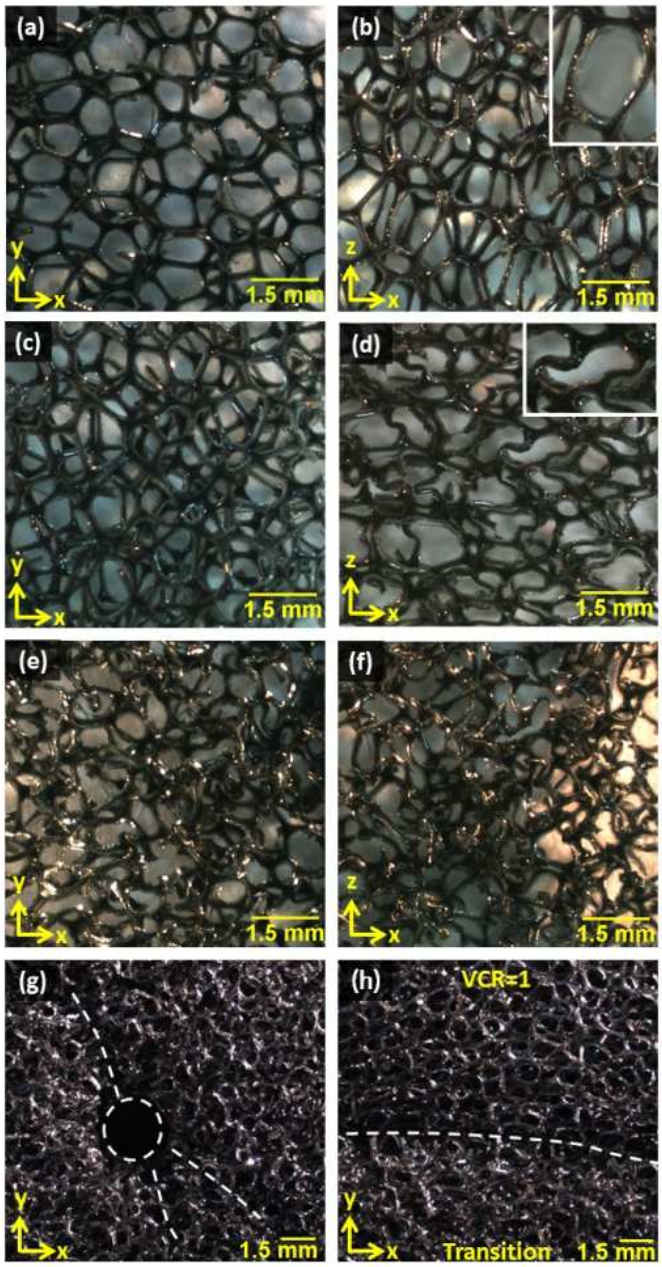

Figure 3: Foam micrographs. Unconverted R30FR foam a) x-y plane and b) x-z plane; VCR = 1 quadrant of gradient sheet c) x-y plane and d) x-z plane; VCR = 2.9 quadrant of gradient sheet e) x-y plane and f) x-z plane; g) Uniform triaxially-compressed auxetic sheet with pin hole and surrounding creases (marked); h) Defined line region between VCR = 1 region (top of image) and higher density transition region (bottom of image) in the gradient sheet (marked). Inserts in b & d include detailed images blown up to 1.5 times the main image.

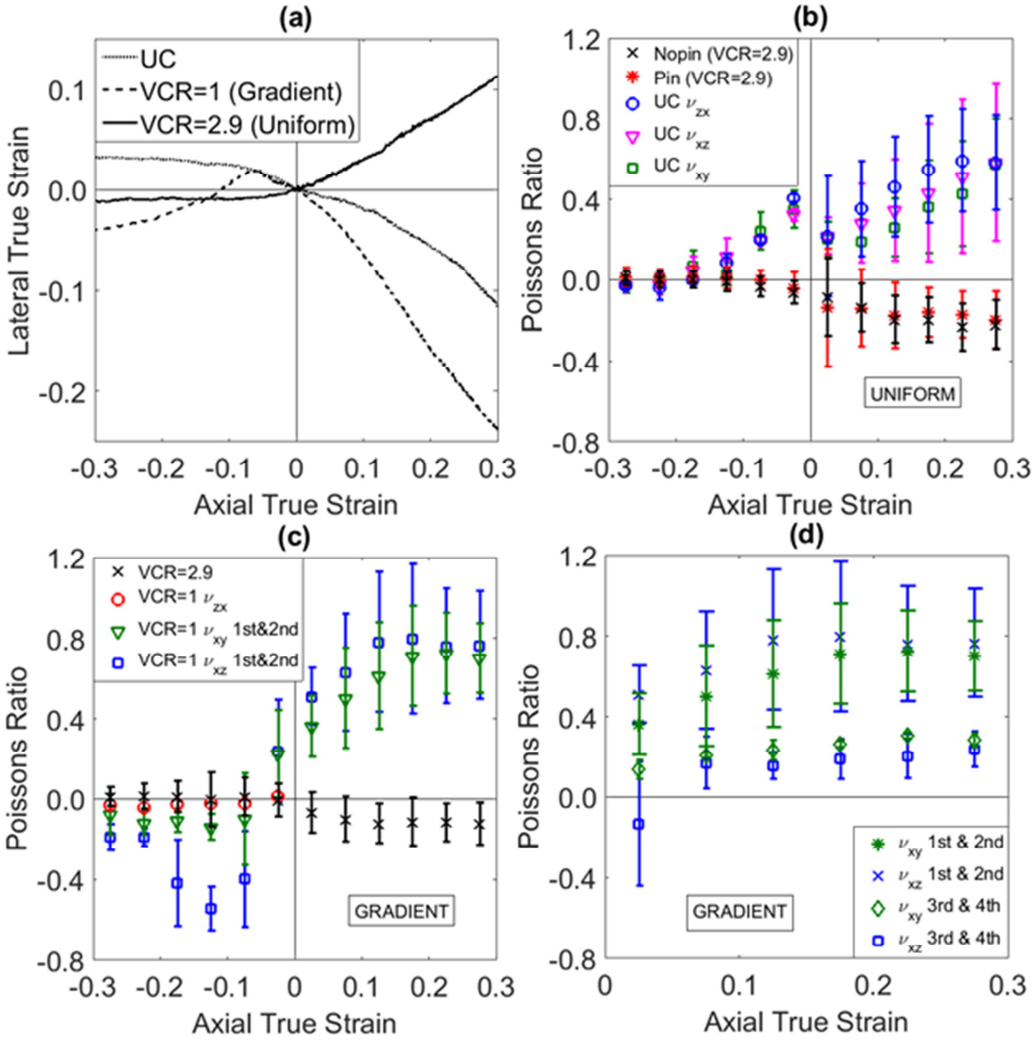

Figure 4: PR responses. a) Lateral vs axial true strain for VCR=2.9 uniform triaxially-compressed sample converted with pins, unconverted (UC) sample and VCR=1 gradient sheet sample, b) PR vs axial true strain for UC and uniform triaxially-compressed samples, c) PR vs axial true strain for gradient sheet samples (VCR=1 tensile data from 1st and 2nd tests performed on each sample – see text) and d) PR vs axial true strain for all tensile tests on VCR=1 region (gradient foam), grouped according to tests 1 and 2, and tests 3 and 4 – see text). Error bars = 1 S.D.

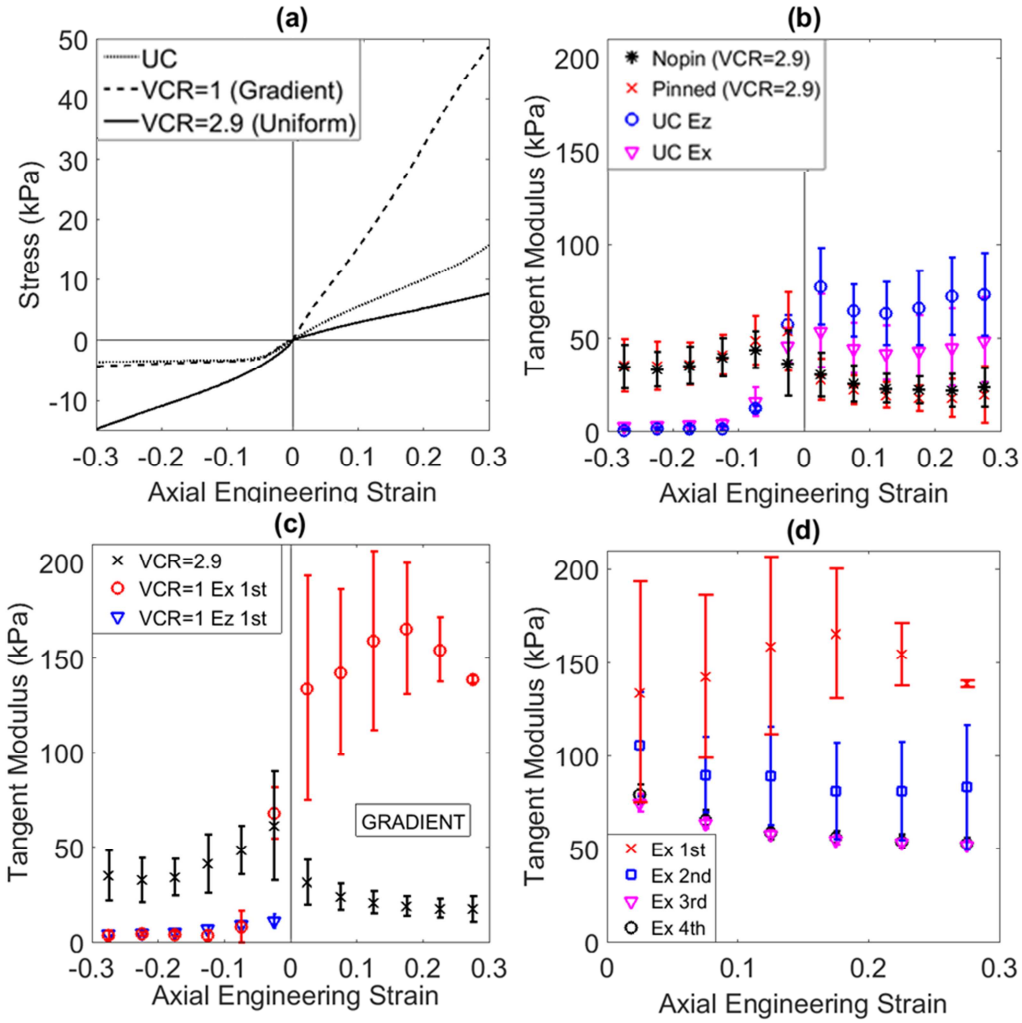

Figure 5: Tangent moduli responses. a) Stress vs axial engineering strain for VCR=2.9 uniform triaxially-compressed sample converted with pins, unconverted (UC) sample and VCR=1 gradient sheet sample, b) Tangent modulus vs axial engineering strain for UC and uniform triaxially-compressed samples, c) Tangent modulus vs axial engineering strain for gradient sheet samples (VCR=1 tensile data from 1st test performed on each sample) and d) Tangent modulus vs axial engineering strain for all tests on VCR=1 region (gradient foam), separated into test number. Error bars = 1 S.D.

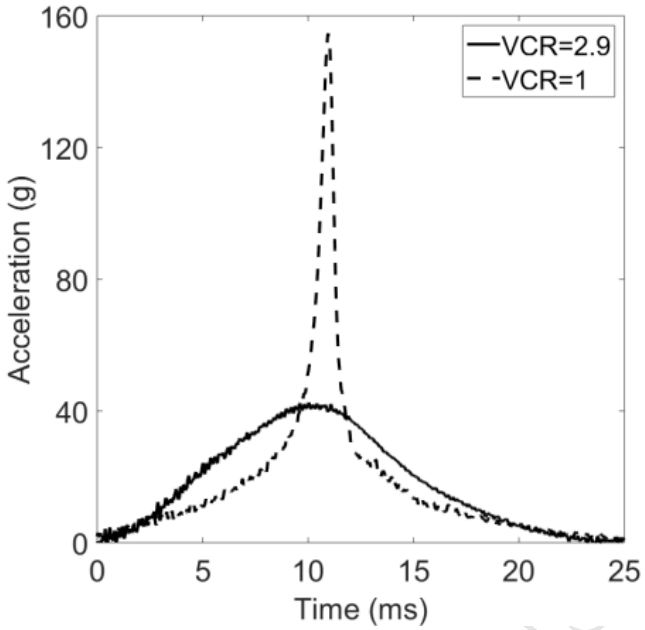

Figure 6: Impact responses. Median acceleration-time traces for the 6J impacts to the gradient sheet impacted through thickness (parallel to the z-axis) in regions with VCR=2.9 and VCR = 1 with the 2 mm PP shell placed on top. Start of impact manually selected at a point when acceleration was greater than 0.

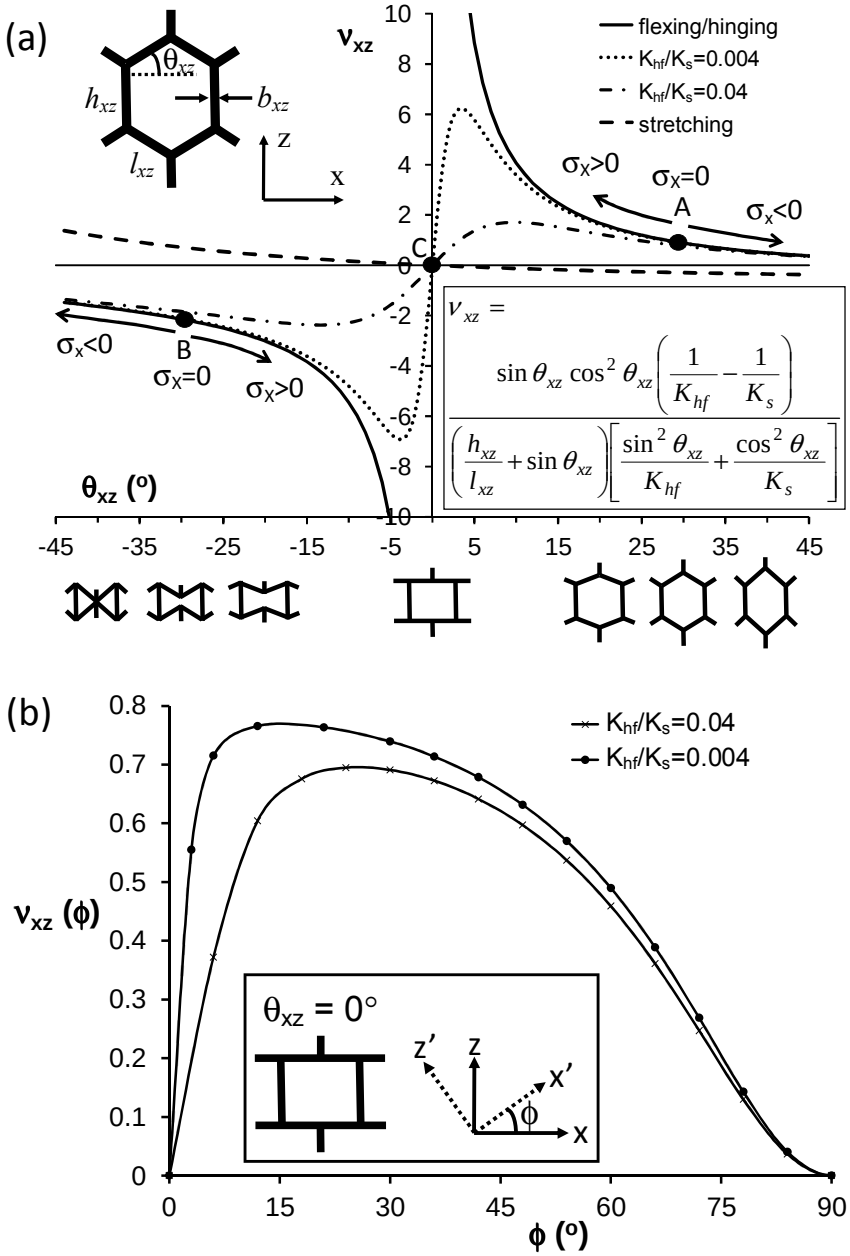

Figure 7: PR vs geometry predictions. (a) ν_{xz} vs θ_{xz} for a honeycomb having h_{xz} = 1.2, l_{xz} = 1, b_{xz} = 0.2 and K_{hf}/K_s = 0 (flexing/hinging), 0.004, 0.04 and ∞ (stretching). Cell geometrical parameters are shown (insert top left), and cell size/shape variation vs θ_{xz} is shown schematically below the figure. (b) ν_{xz} vs φ for the same honeycomb with θ_{xz} = 0 and K_{hf}/K_s = 0.004 and 0.04. Cell shape for θ_{xz} = 0 and definition of rotation angle φ are shown in schematic insert.

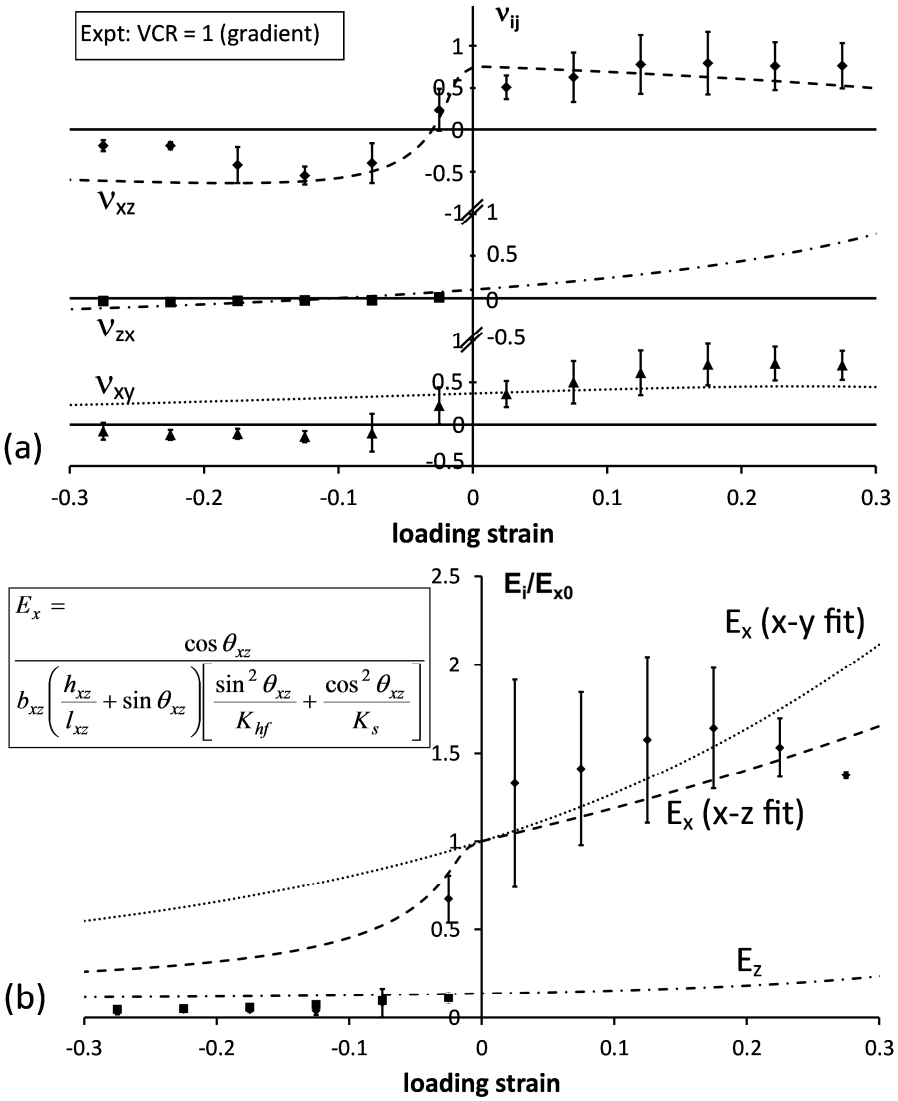

Figure 8: Mechanical properties vs strain predictions. (a) Directional PR predictions (curves) and experimental VCR=1 (gradient foam) data (symbols) vs loading strain: ν_{xz} and ν_{zx} predictions for h_{xz} = 1.2, l_{xz} = 1, b_{xz} = 0.2, θ_{xz} = -0.1°, φ = 10° and K_{hf}/K_s = 0.004 (K_f/K_h = 9, K_s/K_h = 225); ν_{xy} predictions for h_{xy} = l_{xy} = 1, b_{xy} = 0.2, θ_{xy} = 30°, φ = 0° and K_{hf}/K_s = 0.3 (K_f/K_h = 9, K_s/K_h = 3); (b) Directional Young's moduli (normalised to undeformed E_x) predictions (curves) and experimental data (symbols) vs loading strain: model parameters as for (a). The E_x (x-z fit) model expression is shown as an exemplar.